Communications

Study of Precipitation Kinetics in a Super Purity Al-0.8 Pct Mg-0.9 Pct Si Alloy Using Differential Scanning Calorimetry

A.K. GUPTA and D.J. LLOYD

Age-hardenable Al-Mg-Si alloys can provide a wide range of mechanical properties for a variety of commercial applications. These alloys are strengthened by precipitation of the metastable precursors of the equilibrium Mg_2Si (β) phase. The precipitation processes in these alloys have been widely studied, although there are some disagreements regarding the number, structure, and composition of the metastable precipitates formed during aging.[1–7] In addition, there is only limited information available on the initial stages of zone formation and their relationship with the precipitates formed during subsequent aging. There is no doubt that the initial stages of precipitation have significant influence on the aging response of a number of commercial alloys,[8] and understanding the kinetics in the initial stages of precipitation is highly valuable. In this study, the results of such a study on a superpurity-based Al-0.8 pct Mg-0.9 pct Si alloy are reported.

An aluminum alloy containing 0.8 wt pct Mg and 0.9 wt pct Si (in wt pct) was cast as 35 × 230 × 535 mm direct chill (DC) ingot. The ingot was scalped 1/4 mm on each rolling face, homogenized at 560 °C for 6 hours, and hot and cold rolled in several passes to the final thickness of 1.0 mm. Specimens for differential scanning calorimetry (DSC) were punched from the cold-rolled material and subjected to appropriate heat treatments before conducting DSC experiments.

The DSC experiments were carried out in an argon atmosphere using a DU PONT* 2100 instrument equipped with a programmable recorder. For each condition, two runs were carried out under identical conditions.[9] In the first run, pure aluminum discs were placed in both the reference and the sample pans, while in the second run, the aluminum disc in the sample pan was replaced by the specimen. From these two runs, it is possible to determine the heat effects that occurred during heating the alloy in the DSC cell. The rate of heat evolution in the alloy per unit mass, Q, can be expressed as follows:[9]

$$\dot{Q} = \frac{E}{M}\left\{(\dot{q}_2 - \dot{q}_1) - (\dot{q}_2 - \dot{q}_1)_{\dot{Q}=0}\right\} \qquad [1]$$

where M is the mass of the specimen; $\dot{q}_1$ and $\dot{q}_2$ are the heat flows to the reference relative to the sample in runs 1 and 2, respectively; and E is the calibration constant of the calorimeter. The term $(\dot{q}_2 - \dot{q}_1)_{\dot{Q}=0}$ is a small correction factor, which arises due to the differences in the heat capacities of the aluminum and the specimen. To find $\dot{Q}$, the term within the brackets was experimentally determined for each run. The value of the constant E was determined by carrying out calibration runs using an indium standard and was found to be 1.05. The quantity within the brackets of Eq. [1] was experimentally determined for each run and plotted against temperature, as shown in Figure 1. The DSC thermograms were reproducible within an error of 2 °C.

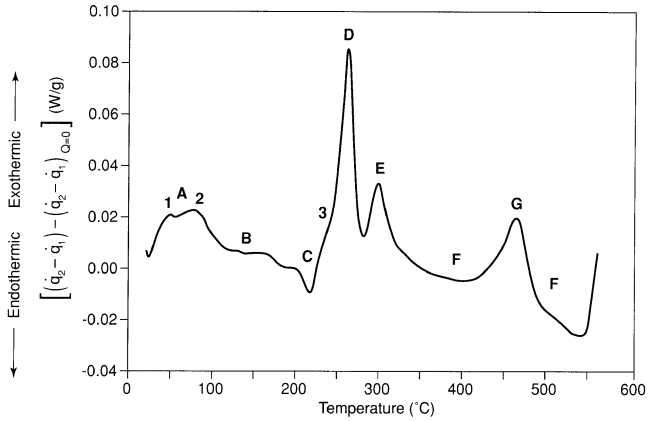

Fig. 1—DSC curve of a superpurity Al-0.8 pct Mg-0.9 pct Si alloy immediately after quenching from solutionizing temperature (at 560 °C). Heating rate: 10 °C/mm

Figure 1 shows a DSC thermogram of the alloy obtained at a heating rate of 10 °C/min immediately after solutionizing at 560 °C for 1 minute and quenching in cold water. The overall shape of the DSC curve is similar to those published in the literature on similar alloys.[3–5,10–17] It can be seen that the precipitation sequence develops in a complicated manner during heating at 10 °C/min. Several reactions occur simultaneously and cause overlapping peaks and troughs in the thermogram. The distinct features of the thermogram in Figure 1 are marked by the letters A through G, while the total heat effects and temperature range are summarized in Table I, along with the proposed reactions associated with each peak based on previous work.[3–5,12–17] There are disagreements in the literature with regard to the specific reaction-peak correspondence, which are a result of the following.

(1) There is disagreement regarding the number, structure, and composition of the metastable phases formed during aging.
(2) There is ambiguity in the nomenclature of different phases. For example, it is not clear whether precluster-ing reactions are independent reactions or are the initial stages of GP(I) zone formation. In addition, sometimes GP(I) zones and GP(II) are also called Mg-Si clusters and β" phases, respectively, while in others, they are considered as different phases.
(3) There is variation in the nature of DSC technique. Under ideal conditions, the total heat effects associated with the precipitation and dissolution reactions should be equal. However, it should be noted that the peaks and troughs in the DSC thermogram do not directly indicate the number of reactions, but reflect the net heat

*Du PONT is a trademark of DuPont de Nemours & Co., Inc., Wilmington, DE.

A.K. GUPTA, Research Scientist, and D.J. LLOYD, Principal Scientist, are with the Kingston Research and Development Centre, Alcan International Limited, Kingston, ON, Canada K7L 5L9.

Manuscript submitted July 21, 1998.

Table I. Analysis of the DSC Curve in Figure 1

Peak/Trough	Total Heat Effect, J/g	Temperature Range, °C		Nature of Peak/Trough		Remarks
		Beginning	End	Subpeak 1	Subpeak 2	
First exothermic peak A	5.7	28.1	116.0	formation of independent clusters of Mg and Si atoms followed by Mg-Si clusters		single peak[3,17]
				Mg-rich Mg-Si clusters		single peak[15]
				GP(I) zones		single peak[5]
				GP(I)	GP(II)/Mg-Si clustering	resistivity data[19,20]
				Preceding reactions are preceded by Si clustering within 2 min of quenching		
				Si-Mg-V	Si-Mg-V	double peak[10,18]
				two types of clusters are formed		
				GP(I)/clustering		single peak[22]
First endothermic trough C	4.5	165.0	230.0	GP(I) dissolution, not studied widely		doublet[5,11,14]
Second exothermic peak D	12.3 (D & E)	230.0	—	GP(I) plus GP(II)/β"		overlapping peak[13]
				β"		single peak[5]
				ordered zones/β"		single peak[16]
				β" and an unknown phase		overlapping peak[3,17]
				β"/GP(II), Si, β'		overlapping peak[11]
Third exothermic peak E	—	—	322.0	β'		single peak[3–5,13,16]
				β plus Si		overlapping[11]
				β		single peak[14]
				β' plus B'		overlapping[3]
				B'		single peak[17]
Second endothermic trough F including peak G	12.9	322.0	553.0	β formation within peak G, the trough F reflects dissolution of precipitates formed earlier		complex reactions[13,15–17]
				β precipitation together with the dissolution of β' and Si*		complex reaction[11]

*(1) β precipitation observed peak E continues beyond 500 °C. (2) Peak G reflects the net effect of redissolution and β precipitation.

flow to the reference, which could be due to one or more reactions. In such situations, identifying peaks unambiguously may be difficult.

With the reference to Figure 1, the decomposition begins with the precipitation reactions under a double peak A, which is followed by a plateau B and a dissolution doublet C. The thermogram clearly shows two precipitation processes, 1 and 2, within the doublet A between 25 °C and 115 °C. The maxima of subpeaks 1 and 2 occur around 50 °C and 75 °C, respectively. The presence of the doublet A in excess Si alloys has been reported prevously[10] and has subsequently been found also in balanced and excess Mg alloys.[18] It should be noted that the precipitation processes within the doublet A are too difficult to resolve by electron-optical techniques and their existence is largely identified from the interpretation of the results obtained from resistivity, chemical composition, and other measurements.[2–4,19–21] To date, there is no general agreement on the identification of subpeaks 1 and 2, although they appear to be linked with two types of clustering reactions. It should be noted from Figure 2 that the Si-Si/Si-Vacancy (V) and Mg-Mg/Mg-V clustering reactions are not observed in as-quenched Al-Si and Al-Mg alloys, respectively. Therefore, it is likely that the two clustering reactions are related to the formation of two types of Mg-Si zones. Recently, Matsuda *et al.*[22] have shown the presence of 2.5-nm-wide, up to 30-nm-long, monolayer thick platelike zones in an Al-1.6 pct Mg_2Si alloy aged at 70 °C for prolonged time. These platelets contain Mg and Si in the ratio of 1:1 and they appear to represent an advanced stage of the two clustering reactions.

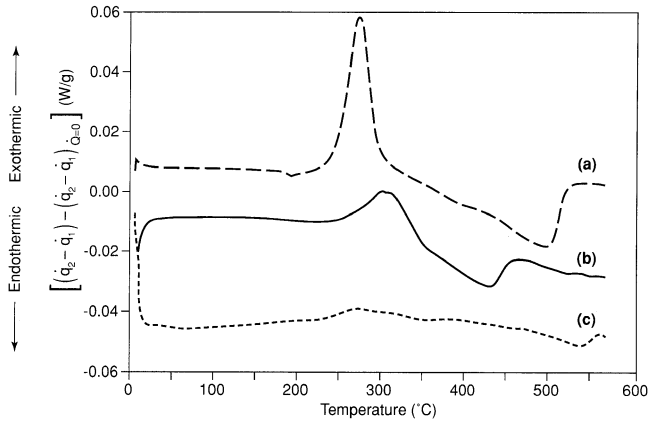

Fig. 2—DSC curves of binary Al-Si and Al-Mg alloys in the solutionized and quenched condition. Heating rate: 10 °C/mm. (*a*) Al-0.9 pct Si, (*b*) Al-0.4 pct Si, and (*c*) Al-2.54 pct Mg.

The peak D with a shoulder marked 3 in Figure 1 may

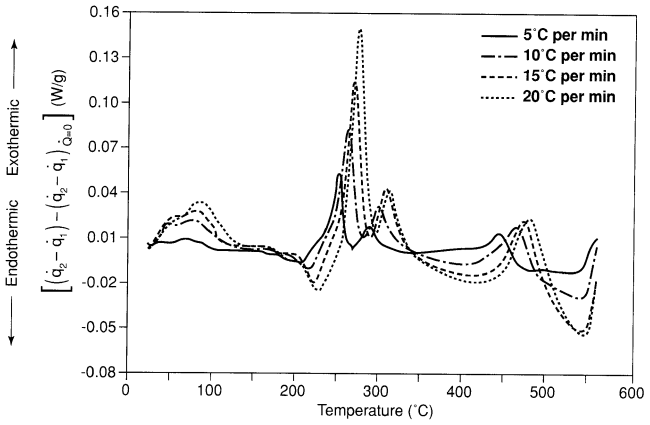

Fig. 3—DSC curves of a superpurity as-quenched Al-0.8 pct Mg-0.9 pct Si alloy at different heating rates.

Table II. Total Heat Effects and Temperature Ranges of the First Precipitation Doublet A at Different Heating Rates

Heating Rate, °C/min	Temperature Range, °C				Total Heat Effect, J/g	f
	Subpeak 1		Subpeak 2			
	Beginning	Maximum	Maximum	End		
5	22.2	35.4	70.5	115.9	5.71	0.77
10	27.4	48.7	75.7	119.1	5.62	0.77
15	30.1	55.3	78.1	129.0	5.9	0.72
20	31.0	56.2	85.3	140.0	5.0	0.71

be considered as representing the formation of three different precipitates, namely, β"/GP(II), β', and Si particles, while peak E is related to the independent precipitation of equilibrium β particles and partial dissolution of β' and finer Si particles.[11]

It should be noted that the processes A and C are related to each other, although they do not overlap in the DSC thermogram, as evidenced by the plateau B. Therefore, it is possible to extract the kinetic information regarding the precipitation processes contributing to Peak A from the DSC data, as shown subsequently.

Figure 3 shows DSC thermograms of the freshly solutionized and quenched alloy at different heating rates. The total heat effects and the characteristics of the peak are listed in Table II. It can be seen that the doublet shifts to higher temperatures with increasing heating rate. This suggests that the processes associated with the doublet are kinetically dominated. The total heat effects and the fractional area, f, of subpeak 2 are (very) similar for the different heating rates, indicating that the equilibrium number of moles of zones forming within the range of the doublet are independent of temperature. Under such conditions, the DSC data can be used to establish the kinetics of the processes associated with the subpeaks 1 and 2.[9]

The mole fraction of precipitates, Y_1, forming under subpeak 1 can be expressed as[8]

$$Y_1 = \frac{A(T)}{A_1} \qquad [2]$$

where $A(T)$ is the area under the doublet between the beginning and the end of a reaction and A_1 is the total area of subpeak 1.

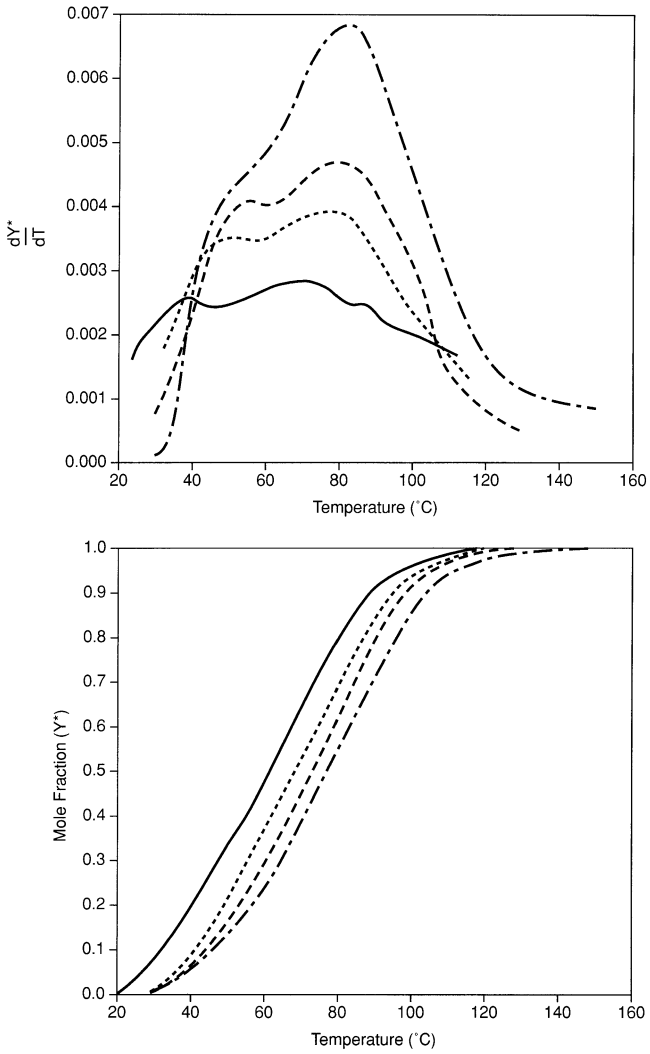

Fig. 4—$\frac{dY^*}{dT}$ *vs* T and Y^* *vs* T plots obtained from the DSC data related to the doublet A in Fig. 3.

If $(A_1 + A_2)$ is the total area under the doublet and the fractional area of subpeak 1 is $(1 - f)$, then Eq. [2] can be written as follows:

$$Y_1 = \frac{Y^*}{(1 - f)} \qquad [3]$$

$$\frac{dY_1}{dT} = \left[\frac{1}{(1 - f)}\right]\left(\frac{dY^*}{dT}\right) = \frac{\left[\left(\dot{q}_2 - \dot{q}_1\right) - \left(\dot{q}_2 - \dot{q}_1\right)_{\dot{Q}=0}\right]}{(1 - f)(A_1 + A_2)} \qquad [4]$$

where

$$Y^* = \frac{A(T)}{(A_1 + A_2)} \qquad [5]$$

The values of Y^* and dY^*/dT in Eqs. [4] and [5] can be experimentally determined from the DSC data in Figure 3 and are plotted in Figure 4.

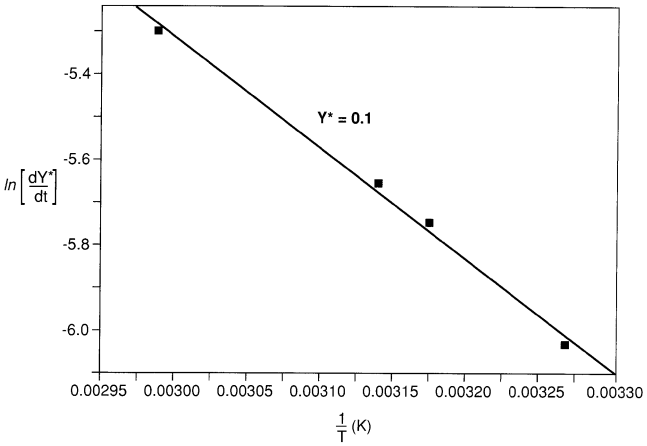

Fig. 5—Activation energy plot for subpeak 1 at a constant value of $Y^* = 0.1$ after Eq. [7].

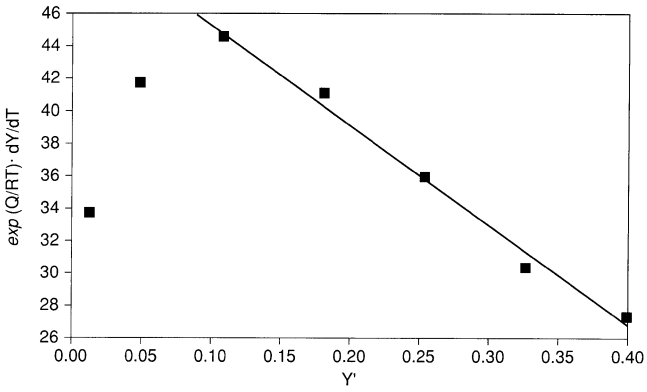

Fig. 6—Plot for the determination of pre-exponential frequency factor K_0 after Eq. [8].

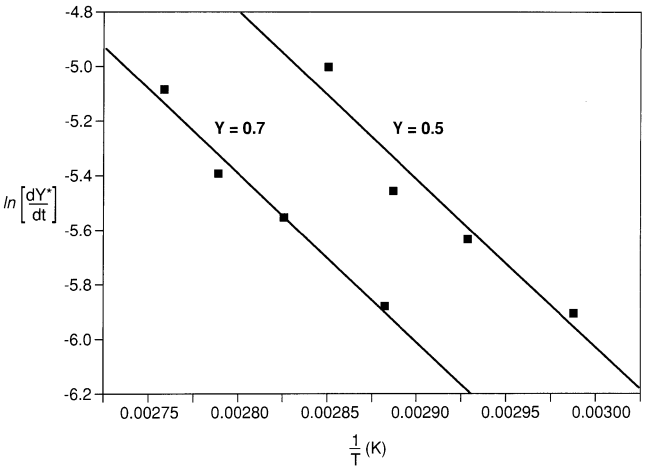

Fig. 7—Activation energy plot for subpeak 2 at $Y^* = 0.5$ and 0.65 after Eq. [9].

The formation of clusters and zones in aluminum alloys is controlled by diffusion, and, therefore, the rate of zone formation, dY/dt, in a nonisothermal DSC run can be expressed as

$$\frac{dY}{dt} = \left(\frac{dY}{dT}\right)\phi = f(Y)k_0 \exp\left(-\frac{Q^*}{RT}\right) \qquad [6]$$

where Y is the mole fraction of precipitates, ϕ is the heating rate, k_0 is the frequency factor, Q^* is the activation energy, R is the universal gas constant, T is the temperature, and $f(Y)$ depends on Y only.

For subpeak 1, Eqs. [3] through [6] can be rearranged to give

$$\ln\left[\left(\frac{dY^*}{dt}\right)_{Y^{*'}}\right] = \ln\left[(1-f)k_0 f\left(\frac{Y^*}{(1-f)}\right)\right] - \frac{Q^*}{R}\left(\frac{1}{T_j}\right) \qquad [7]$$

where ϕ is the heating rate, $(dY^*/dt)_{Y^{*'}}$ is the rate of transformation at a fixed value of Y^* at different heating rates, and T_j is the temperature at $Y^{*'}$ for jth heating rate. A plot after Eq. [7] will be a straight line and the slope will yield a value of activation energy of the process related to subpeak 1. The data in Figure 4 are plotted in Figure 5 after Eq. [7] for a constant value of $Y^* = 0.10$ within the range of the subpeak 1. The least-squares fit of the data in Figure 5 yields an activation energy of 24.9 kJ/mole, which is considerably lower than expected for cluster formation. The asquenched microstructure of Al-Mg-Si alloys does not show many dislocation loops, suggesting that the excess vacancies are associated with Mg and Si solute atoms. In addition, the interaction energy between Mg and Si atom is high and reduces the energy required for diffusion to form clusters and zones.[13] This may explain why the activation energy determined in this study is lower than those reported for the GPB zones in an Al-Cu-Mg alloy by Jena *et al.*[9]

The value of the pre-exponential frequency factor k_0 in Eq. [6] was determined by appropriate substitutions and assuming $f(Y) = (1 - Y)$, as follows:

$$\left(\frac{dY^*}{dT}\right)e^{\frac{Q^*}{RT}} = C - \left(\frac{k_0}{\phi}\right)Y^* \qquad [8]$$

where C is a constant. The plot after Eq. [8] will yield a straight line provided the assumption regarding the form of function $f(Y)$ is valid and the slope will equal the frequency factor k_0. It should be noted that the scatter in the value of k_0 was considerable at different heating rates, which is largely due to the limited data related to Y^* and dY^*/dT for subpeak 1. Figure 6 shows the plot obtained for a 5 °C/min heating rate, and the slope gives a value of $k_0 = 70$. This value is also much lower than expected for zone forming processes.[9] The lower k_0 and Q^* values suggest that the subpeak 1 process starts and finishes very rapidly, consistent with the fact that the subpeak 1 disappears within an hour of quenching.

The kinetic analysis of the subpeak 2 can be carried out in the same manner as that used for subpeak 1. For subpeak 2, Eq. [7] becomes

$$\ln\left[\left(\frac{dY^*}{dt}\right)_{Y^{*'}}\right] = \ln\left\{fk_0\left[\frac{(Y^{*'}-1)}{f}+1\right]\right\} - \frac{Q^*}{R}\left(\frac{1}{T_j}\right) \qquad [9]$$

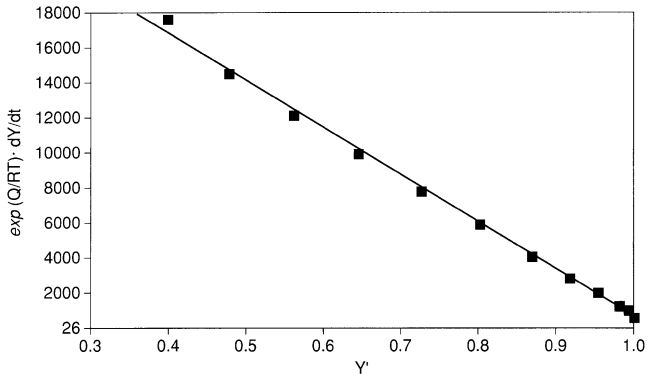

Fig. 8—Plot to determine the value of pre-exponential frequency factor K_0 after Eq. [8].

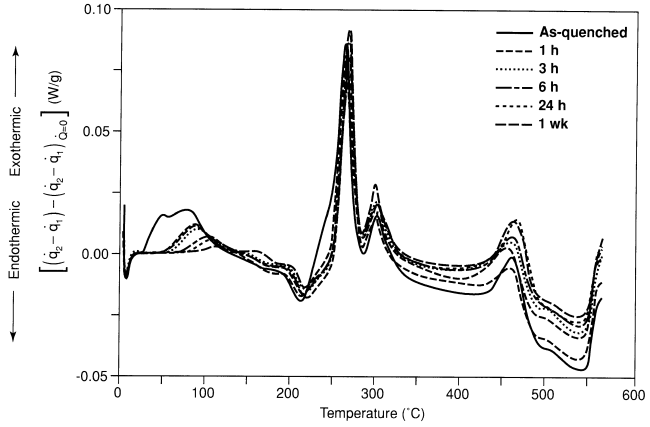

Fig. 9—Effect of natural aging on the thermogram of as-quenched Al-0.8 pct Mg-0.9% Si alloy.

Figures 7 and 8 show plots after Eqs. [9] and [6], respectively, for determination of the activation energy and the frequency term for the process associated with the subpeak 2. It can be seen that the plots in both figures are linear and their slopes give the values of 44.4 kJ/mole and 3×10^4 for the activation energy and pre-exponential factors, respectively. The activation energy for subpeak 2 is close to the values reported by Kovacs *et al.*[20] and Dutta *et al.*[12,13] in as-quenched, superpurity Al-0.85 pct Mg_2Si and AA6061 alloys.

It seems that the subpeak 2 process represents an advanced stage of subpeak 1. A few studies have reported the occurrence of the Si-clustering during or shortly after quenching (15 and 19 to 20 pct). The reaction occurs too fast to record on a DSC thermogram (Figure 2). Therefore, it is possible that the zones formed in subpeak 1 are Mg-Si (rich) clusters, which become Mg-Si (depleted) clusters in subpeak 2. The later process proceeds slowly and is not completed even after 1 week of natural aging (Figure 9). Table III summarizes the results of the kinetic analysis of subpeaks 1 and 2 and highlights the effect of natural aging on both kinetics and the precipitation process. Table III shows that the subpeak 2 temperature range shifts to higher temperature with natural aging, although the shape of the DSC curve is not affected significantly. The activation energy associated with subpeak 2 is increased with natural aging, which is consistent with the measurements on AA6061 by Dutta *et al.*[12,13]

The aging process in an as-quenched superpurity Al-0.8 pct Mg-0.9 pct Si alloy proceeds with the formation of clusters and zones, followed by sequential precipitation of other metastable phases, Si and B precipitates. The DSC thermogram of the as-quenched material is very complicated due to the appearance of overlapping peaks caused by simultaneous precipitation and dissolution reactions. Therefore, the precipitation kinetics associated with the different stages of aging is difficult to establish. However, in the initial stages of precipitation, the different precipitation and dissolution reactions do not overlap extensively, and it is possible to establish the kinetics.

The initial stages of precipitation are characterized by two clustering reactions represented by subpeaks 1 and 2 in the 25 °C to 120 °C range of a thermogram obtained at 10 °C/min. The clustering reaction associated with subpeak 1 is complete within 1 hour of quenching, and the precipitation kinetics of subpeak 1 can be expressed by the equation

$$\frac{dY}{dt} = \left(\frac{dY}{dT}\right)\phi = (1 - Y) * 70 * \exp\left(-\frac{3000}{T}\right)$$

The formation of subpeak 2 is characterized by diffusion of Mg atoms into the Si-rich Mg-Si clusters and forms Si depleted Mg-Si clusters. This process occurs slowly and continues for more than a week at room temperature. During heating, the peak associated with subpeak 2 is shifted to higher temperatures with natural aging, and the precipitation kinetics of the subpeak 2 can be expressed as follows;

$$\frac{dY}{dt} = \left(\frac{dY}{dT}\right)\phi = (1 - Y) * 3 * 10^4 * \exp\left(-\frac{5340}{T}\right)$$

Table III. Kinetic Parameters Associated with the First Precipitation Doublet Aging Process and Effect of Natural Aging on the Kinetics Heating Rate 10 °C/min

		Peak Temperature, °C					
Aging Time, h	Total Heat Effect, J/g	Beginning	Maximum	End	$f(Y)$	k_0/s	Q, KJ/mole
0	5.62	27.4	—	119.1	$(1 - Y)$	70	24.9 subpeak 1
1	3.87	35.1	—	139	$(1 - Y)$	3×10^4	44.4 subpeak 2
3	2.79	45.1	—	134.9	$(1 - Y)$	2.5×10^7	66.0
6	2.33	50.0	—	139.9	—	—	—
24	1.49	60.2	—	139.1	$(1 - Y)$	8×10^7	71.0
72	1.14	70.1	—	144.9	—	—	—
1 week	1.13	75.0	—	175	—	—	—

The value of activation energy increases with an increase in natural aging after quenching.

The authors thank Professor A.K. Jena, Visiting Professor at the Department of Mechanical and Industrial Engineering, University of Manitoba (Winnipeg, MB, Canada), for the valuable discussion. The technical support of Justine Bookbinder is also greatly appreciated.

REFERENCES

1. K. Matsuda, S. Ikeno, T. Sato, and A. Kamio: *Mater. Sci. Forum*, 1996, vols. 217–222, pp. 707-12.
2. G.A. Edwards, K. Stiller, and G.L. Dunlop: *Appl. Surf. Sci.*, 1994, vol. 76/77, pp. 219-25.
3. G.A. Edwards, M.J. Couper, and G.L. Dunlop: in *Aluminum Alloys: Their Physical and Mechanical Properties ICAA4*, T.H. Sanders, Jr. and E.A. Starke, Jr., The Georgia Institute of Technology, Atlanta, GA, 1994, pp. 620-27.
4. G.A. Edwards, K. Stiller, G.L. Dunlop, and M.J. Cooper: *Acta Metall.*, 1998, vol. 46 (11), pp. 3893-3904.
5. N. Maruyama, R. Uemori, N. Hashimoto, M. Saga, and M. Kikuchi: *Scripta Metall.*, 1997, vol. 36 (1), pp. 89-93.
6. J.P. Lynch, L.M. Brown, and M.H. Jacobs: *Acta Metall.*, 1982, vol. 30, pp. 1389-95.
7. P. Donnadieu and A. Proult: *Mater. Sci. Forum*, 1996, vols. 217–222, pp. 719-24.
8. P.E. Fortin: *Can. Met. Quart.*, 1963, vol. 2, pp. 143-55.
9. A.K. Jena, A.K. Gupta, and M. Chaturvedi: *Acta Metall.*, 1989, vol. 37 (3), pp. 885-95.
10. A.K. Gupta and D.J. Lloyd: in *Aluminum Alloys: Their Physical and Mechanical Properties*, ICAA3, L. Arnberg, O. Lohne, E. Nes and N. Ryum, eds., The Norwegian Institute of Technology, Trondheim, Norway, 1992, vol. 2, pp. 21-25.
11. A.K. Gupta and D.J. Lloyd: *Recent Metallurgical Advances in Light Metal Industries*, CIM Conf., Vancouver, S. MacEwen and J.P. Gilordeau, eds., The Canadian Institute of Mining, Metallurgy and Petroleum, Montreal, Canada, 1995, pp. 243-53.
12. I. Dutta, S.M. Allen, and J.L. Hafley: *J. Mater. Sci. Lett.*, 1991, vol. 10, pp. 323-26.
13. I. Dutta, S.M. Allen, and J.L. Hafley: *Metall. Trans. A*, 1991, vol. 22A, pp. 2553-63.
14. C. Badini, F. Marino, and A. Tomasi: *J. Mater. Sci.*, 1991, vol. 26, pp. 6279-87.
15. P. Barczy and F. Trainta: *Scand. J. Metall.*, 1975, vol. 4, pp. 284-88.
16. T. Hirata and S. Matsuo: *Trans. Jpn. Inst. Metall.*, 1971, vol. 12 (2), pp. 101-106.
17. L. Zhen, W.D. Fei, S.B. Kang, and H.W. Kim: *J. Mater. Sci.*, 1997, vol. 32, pp. 1895-902.
18. M. Takeda, F. Ohkubo, T. Shirai, and K. Fukai: *Mar. Sci. Forum*, 1996, vols. 217–222, pp. 815-20.
19. A. Lutts: *Acta Metall.*, 1961, vol. 9, pp. 577-86.
20. I. Kovacs, J. Lendvai, and E. Nagy: *Acta Metall.*, 1972, vol. 20 (7), pp. 975-83.
21. U. Schmidt, M. Joachimi, L. Petzold, and F. Eichhorn: *Cryst. Res. Technol.*, 1984, vol. 19, vol. 7, pp. 981-89.
22. K. Matsuda, H. Gamada, K. Fujii, Y. Uetani, T. Sato, A. Kamis, and S. Ikeno: *Metall. Mater. Trans. A*, 1998, vol. 29A, pp. 1161-67.

Kinetics of Homogeneous Martensitic Nucleation in Iron-Based Alloys

X.Q. ZHAO and Y.F. HAN

Based on small particle experiments,[1] Cech and Turnbull proposed the concept of heterogeneous nucleation of martensitic transformation. Later, Kaufman and Cohen[2] estimated the critical free energy for homogeneous nucleation, and pointed out that the energetic nucleation barrier is much higher than the energy involved in thermal fluctuation, and the possibility of homogeneous nucleation thereby can be ruled out. On this basis, Cohen and co-workers developed heterogeneous models based on pre-existing embryos and dislocations, respectively.[2,3] Later, some investigators employed quantitative crystallography approaches to study the nucleation kinetics of iron-based alloys, particularly of Fe-Ni-Mn alloys exhibiting isothermal transformation kinetics mode,[4–11] indicating that the heterogeneous nucleation activation energy is much less than the homogeneous nucleation work obtained by the estimation by Kaufman and Cohen.[2] These experimental investigations seem to be compatible with the heterogeneous nucleation mechanism and deny the possibility of homogeneous nucleation mode. In order to solve the problems associated with martensitic nucleation, especially to explain such low activation energy for nucleation, several models have been proposed to attempt to account for the mechanism of heterogeneous nucleation of martensitic transformation,[3–5,12,13] although so far these models have not been confirmed directly by experiments. Of these models, the most prevailing is the one proposed by Olson and Cohen on the basis of special configurations of dislocations, improbable defects.[3] However, recent experiments by Kajiwara[14] and Kajiwara[15] demonstrated that dislocations could not serve as favorable sites for martensitic nucleation and that the Bogers–Burgers shear mechanism, as a basis of the model by Olson and Cohen, is not suitable for explanation of martensitic transformation. Furthermore, computer simulation and experimental results of ultrafine iron-based alloy particles indicated that martensitic transformation may occur in perfect crystals containing no dislocation.[16,17,18] Very recently, the present authors re-evaluated the nucleation work for martensitic transformation, suggesting that the homogeneous nucleation in iron-based alloys is thermodynamically permitted.[19] Following this consideration, the present article will be concerned with the kinetic aspects of homogeneous martensitic nucleation in iron-based alloys, of which many experiments have been carried out and plenty of data are available associated with the kinetics of martensitic transformation in various iron-based alloys.

According to classical nucleation theory,[2] the nucleation energy (ΔW) for forming a martensitic nucleus in a shape of oblate spheroid of radius r and semithickness c in a homogeneous matrix can be given by

X.Q. ZHAO, Associate Professor, and Y.F. HAN, Professor, are with No. 14 Department, Beijing Institute of Aeronautical Materials, 100095 Beijing, People's Republic of China.

Manuscript submitted June 23, 1998.